



WO₃ monolayer loaded on ZrO₂: Property–activity relationship in *n*-butane isomerization evidenced by hydrogen adsorption and IR studies

Ainul Hakimah Karim^a, Sugeng Triwahyono^{a,*}, Aishah Abdul Jalil^b, Hideshi Hattori^c

^a Ibnu Sina Institute for Fundamental Science Studies, Faculty of Science, Universiti Teknologi Malaysia, 81310 UTM Johor Bahru, Johor, Malaysia

^b Institute of Hydrogen Economy, Faculty of Chemical Engineering, Universiti Teknologi Malaysia, 81310 UTM Johor Bahru, Johor, Malaysia

^c Catalysis Research Center, Hokkaido University, Sapporo 011-0021, Japan

ARTICLE INFO

Article history:

Received 28 February 2012

Received in revised form 11 April 2012

Accepted 29 April 2012

Available online 9 May 2012

Keywords:

WO₃–ZrO₂

Protonic acid sites

Lewis acid sites

Hydrogen uptake

n-Butane isomerization

ABSTRACT

The property–activity relationship of WO₃ supported on ZrO₂ (WZ) was evaluated in *n*-butane isomerization for a series of catalysts with WO₃ loading ranging from 5 to 20 wt% on ZrO₂. The catalysts were prepared by incipient-wetness impregnation of Zr(OH)₄ with an aqueous solution of (NH₄)₆[H₂W₁₂O₄₀·*n*H₂O], followed by drying and calcination at 1093 K. The introduction of WO₃ continuously increased the tetragonal phase of ZrO₂, WO₃ surface density and coverage. The specific surface area and total pore volume passed through a maximum of WO₃ loading at 13 wt%; this loading corresponds to 5.9 WO₃/nm² and is near the theoretical monolayer-dispersed limit of WO₃ on ZrO₂. The IR results indicate that the presence of WO₃ eroded the absorbance bands at 3738 and 3650 cm⁻¹ corresponding to bibridged and tribridged hydroxyl groups up to near the monolayer-dispersed limit of WO₃. A new broad and weak band appeared, centered at 2930 cm⁻¹, indicating the presence of bulk crystalline WO₃ for WO₃ coverage exceeding the theoretical monolayer-dispersion limit. In addition to the band at 2930 cm⁻¹, two W=O stretching bands were observed at about 1021 and 1014 cm⁻¹ for all WZ catalysts, confirming the existence of W=O connected to coordinative unsaturated (cus) Zr⁴⁺ through O and to the other W through O, respectively. Pyridine adsorbed IR and NH₃-TPD revealed that the presence of WO₃ modified the nature and concentration of acidic sites. The highest acidity was observed with 13 wt% loading WO₃. The decrease in the intensity of peaks due to increasing WO₃ loading was much higher on Lewis acid sites than on Brønsted acid sites. Hydrogen adsorption isotherms and the IR results for hydrogen adsorption on preadsorbed pyridine were used to evaluate the formation of active protonic acid sites from molecular hydrogen. The catalyst with 13 wt% WO₃ loading showed the maximum hydrogen uptake capacity and formation of protonic acid sites. These results show a direct correlation with the activity of WZ in *n*-butane isomerization at 573 K in which 13 wt% WO₃ loading on ZrO₂ yielded the highest amount of isobutane. It is suggested that the presence of strong Lewis acid sites on monolayer-dispersed WO₃ facilitates the formation of protonic acid sites from hydrogen in the gas phase which act as active sites in *n*-butane isomerization. The presence of permanent Brønsted acid sites could not be directly associated with activity. In fact, no isomerization activity was observed in the absence of hydrogen.

© 2012 Elsevier B.V. All rights reserved.

1. Introduction

Zirconia-based solid acid catalysts such as SO₄²⁻–ZrO₂ (SZ), MoO₃–ZrO₂ (MZ) and WO₃–ZrO₂ (WZ) catalysts have been explored widely due to their potential for replacing halide-type solid acids and zeolite for linear alkane isomerization [1–7]. Skeletal isomerization over solid acid catalysts is normally carried out in the presence of hydrogen. Without hydrogen, catalytic activity decreases rapidly with the reaction time due to the formation

of coke deposits and/or the lack of active sites for isomerization. Our research group has studied the effects of hydrogen on the catalytic activities of SZ, MZ and WZ catalysts for acid-catalyzed reactions [8–10]. Our results suggest that protonic acid sites are generated from molecular hydrogen and act as catalytically active sites, not only for the skeletal isomerization of alkanes, but also for acid-catalyzed reactions such as cumene cracking and toluene disproportionation. On the basis of pyridine adsorbed IR, hydrogen adsorbed ESR and quantitative hydrogen adsorption studies, we have proposed the concept of “molecular hydrogen-originated protonic acid sites” that involves the generation of protonic acid sites on the surface of solid acid materials from molecular hydrogen [9–13]. Hydrogen molecules are dissociatively adsorbed on specific

* Corresponding author. Tel.: +60 7 5536076; fax: +60 7 5536080.
E-mail addresses: sugeng@utm.my, sugengtw@gmail.com (S. Triwahyono).

active sites to form hydrogen atoms, followed by spillover onto the support and surface diffusion. Each spillover hydrogen atom reaches a Lewis acid site and donates an electron to form H^+ . H^+ is then stabilized on an O atom near the Lewis acid site. The Lewis acid site trapped electron reacts with a second spillover hydrogen to form H^- bound to a Lewis acid site.

Recently, several research groups have extensively focused on the study of WZ catalysts, as they are more thermally and chemically stable catalysts compared to SZ and MZ catalysts. WZ catalysts do not suffer from tungsten loss during thermal treatment, undergo significantly less deactivation during the reaction and can be operated at relatively high temperatures with higher selectivity and fewer cracking products. The amount of tungsten loading has become an interesting topic of discussion as the properties and activities of WZ are strongly determined by W loading. There seems to be a general consensus in the literature that the maximum activity of WZ is achieved with near monolayer surface tungsten oxide coverage of ZrO_2 catalysts, although the number of W atoms required to form a monolayer is dependent on the configuration of surface polytungstate on the ZrO_2 surface. Scheithauer et al. have reported that Brønsted acid site strength increases with increasing WO_3 loading up to saturation and remains constant at higher loading in which the strength of these permanent Brønsted acid sites determines the activity of WZ in *n*-pentane isomerization [14]. Similarly, Naito et al. have concluded that the Brønsted acid sites on monolayer-dispersed WO_3 ($\cong 6.4$ W atoms/ nm^2) are active for the isomerization of *n*-butane [15]. They have stated that the maximum activity at 6.4 W atoms/ nm^2 is in good agreement with the maximum Brønsted acidity of the catalyst. Further WO_3 loading diminishes the activity of both Lewis and Brønsted acid sites. Lebarbier et al. studied the properties and catalytic performance of WZ in 2-propanol dehydration and *n*-hexane isomerization [16]. They concluded the presence of threshold of W surface density for 2-propanol dehydration (1.3 W/ nm^2) and *n*-hexane isomerization (3.4 W/ nm^2). The difference in the minimum W loading required for the development of activity for both reactions was attributed to the necessity of stronger Brønsted acid sites for the *n*-hexane isomerization. In addition, a direct relationship of the permanent Brønsted acid site and catalytic activity for 2-propanol dehydration was observed. Whereas, the presence of hydrogen in gas phase is required in the activation of catalyst and isomerization of *n*-hexane at

for WZ catalysts. They found that the activity of a WZ catalyst in *n*-pentane isomerization was lower than that of zeolite or SZ catalysts, although the WZ catalyst possessed higher acidity than zeolite or the SZ catalysts [19].

Although numerous published studies have been devoted to the establishment of the properties and activity of WZ catalysts, reports showing direct evidence for the property–activity relationship of WZ catalysts have been lacking. In particular, the effects of tungsten loading have only been evaluated on the basis of physical properties, acidity and catalytic activities. In the present study, we demonstrate the results of IR studies of hydrogen adsorption on pyridine together with isothermal hydrogen uptake results and the catalytic isomerization of *n*-butane in order to clarify the relationship between WO_3 loading with the formation of active protonic acid sites, hydrogen uptake and the activity of WZ catalysts. The results indicate that 13WZ, which possessed the strongest Lewis acid sites, had greatest ability and capacity to form and to take up active protonic acid sites from molecular hydrogen. In the presence of hydrogen in the gas phase, the activity of the catalyst in *n*-butane isomerization passed through a maximum at 13 wt%, showing a direct relationship between hydrogen uptake and the activity of the catalyst, whereas the presence of permanent Brønsted acid sites could not be directly associated with activity. In fact, no activity was observed for *n*-butane isomerization in the absence of hydrogen.

2. Experimental

2.1. Preparation of catalyst

Zirconium hydroxide ($Zr(OH)_4$) was prepared from an aqueous solution of $ZrOCl_2 \cdot 8H_2O$ (Wako Pure Chemical) by hydrolysis with 2.8 wt% NH_4OH aqueous solution [20]. The final pH value of the supernatant was 9.0. The precipitate was filtered and washed with deionized water. The gel obtained was dried at 383 K to form $Zr(OH)_4$. Tungstated zirconia (WZ) with various weight percentages of WO_3 were prepared by incipient-wetness impregnation of $Zr(OH)_4$ with aqueous solution of $(NH_4)_6[H_2W_{12}O_{40} \cdot nH_2O]$, followed by drying at 383 K overnight and calcination at 1093 K for 3 h in air. 5, 10, 13, 15 and 20 wt% WO_3 supported on ZrO_2 were prepared and the catalysts are denoted as [wt%]WZ, where [wt%] indicated the wt% of WO_3 on WZ catalyst.

The surface density of WO_3 , ρ_{WO_3} is determined by Eq. (1) [10].

$$\rho_{WO_3} \left[\frac{WO_3 \text{ atoms}}{nm^2 \text{ sample}} \right] = \frac{wt\% \text{ } WO_3 / 100 [g \text{ } WO_3 / g \text{ sample}] \times 1 / MW_{WO_3} [mol \text{ } WO_3 / g \text{ } WO_3] \times N_A [WO_3 \text{ atoms/mol } WO_3]}{SA_{\text{sample}} [nm^2 \text{ sample/g sample}]} \quad (1)$$

523 K. Soultanidis et al. has explored the effect of tungsten surface density in the properties and catalytic activity of *n*-pentane isomerization [17]. They concluded that the surface Brønsted acidity of WZrOH sample treated at 973 K was constant at ~ 0.035 sites/W-atom below monolayer dispersed W and decreased gradually above monolayer dispersed W. However the activity of WZrOH samples demonstrated a volcano-shape dependence on tungsten surface density with maximum activity at 5.2 W/ nm^2 due to the large population of Zr– WO_x clusters. Barton et al. have concluded that a large polytungstate species is required to delocalize the negative charge counterbalancing the formation protonic species from hydrogen in the gas phase in which the protonic species increase isomerization and prevent deactivation [18]. The maximum *o*-xylene isomerization turnover rates were obtained at WO_x surface densities of 10 W atoms/ nm^2 , which exceeds the theoretical monolayer capacity of ZrO_2 . Even though most of these reports agree with the acidic property–catalytic activity relationship of solid acid catalysts, Vartuli et al. have suggested that the comparisons of catalytic activity between materials based entirely on acid strength may not be valid

where W_{WO_3} , MW_{WO_3} , N_A and SA are the weight of WO_3 per unit weight of catalyst, molecular weight of WO_3 , Avogadro number and the surface area of catalyst, respectively.

The theoretical WO_3 surface coverage, θ_{WO_3} is determined by Eq. (2).

$$\theta_{WO_3} = \rho_{\text{surf}} \left[\frac{WO_3 \text{ atom}}{nm^2 \text{ support}} \right] \times A_{WO_3} \left[\frac{nm^2 \text{ } WO_3}{WO_3 \text{ atom}} \right] \quad (2)$$

where A_{WO_3} is the molecular area of WO_3 which was determined from the bulk density of WO_3 .

2.2. Characterization of catalyst

The crystalline structure of catalysts was determined with XRD recorded on a Bruker AXS D8 Automatic Powder Diffractometer using Cu $K\alpha$ radiation with $\lambda = 1.5418 \text{ \AA}$ at 40 kV and 40 mA, over the range of $2\theta = 20\text{--}40^\circ$. The fraction of tetragonal and monoclinic

phase of ZrO_2 in the catalyst was determined based on the formula proposed by Toraya et al. [21].

$$V_t = 1 - \frac{1.31X_m}{1 + 0.31X_m} \quad (3)$$

$$X_m = \frac{I_m(1\ 1\ \bar{1}) + I_m(1\ 1\ 1)}{I_m(1\ 1\ \bar{1}) + I_m(1\ 1\ 1) + I_t(1\ 1\ 1)} \quad (4)$$

where X_m is the intensity ratio of monoclinic of ZrO_2 . $I_t(1\ 1\ 1)$, $I_m(1\ 1\ 1)$ and $I_m(1\ 1\ \bar{1})$ are the integrated intensity of the (111) reflection of the tetragonal phase at $2\theta = 30.2^\circ$, (111) reflection of the monoclinic phase at $2\theta = 31.8^\circ$ and (11 $\bar{1}$) reflection of the monoclinic phase of zirconia at $2\theta = 28.2^\circ$, respectively. While, 1.31 is Toraya's theoretical deviation from the linearity value.

The specific surface area and BJH pore size distribution of the catalyst were determined with a Quantachrome Autosorb-1 at 77 K. Prior to the analysis, the catalyst was outgassed at 573 K for 3 h.

Temperature-programmed desorption of ammonia (NH_3 -TPD) was carried out with ThermoQuest TPD1100 by a procedure similar to that described in previous report [2]. In brief, the catalyst was activated with hydrogen flow at 673 K for 3 h followed by purging with He flow at 673 K for 30 min, to ensure the removal of adsorbed water and organic contaminants. Then, the activated catalyst was exposed to 10 Torr of dehydrated ammonia at 373 K for 30 min followed by purging with He flow at 373 K for 30 min. The TPD was run at a heating rate of 10 K/min from room temperature to 1200 K under the He flow, and the desorbed ammonia was detected by mass spectrometry. In the measurement of IR spectra, a self-supported wafer placed in an in situ stainless steel IR cell with CaF_2 windows was activated with a hydrogen flow at 623 K for 3 h, followed by outgassing at 623 K for 2 h [22,23]. The sample was exposed to 0.13 kPa of pyridine at 423 K, followed by outgassing at 573 K. In the H_2 -exposure process, pyridine was adsorbed on activated sample at 423 K and outgassed at 573 K followed by exposure of dried hydrogen (13.35 kPa) at room temperature. The catalyst then was heated stepwise from room temperature in 50 K increments to 523 K for 30 min each. Since the catalysts have been activated with hydrogen at 623 K, the catalysts will not be reduced further on contact with hydrogen at a temperature 523 K and below. All spectra were recorded on a Perkin-Elmer Spectrum GX FT-IR Spectrometer at room temperature.

2.3. Isothermal hydrogen adsorption

Isothermal hydrogen uptake was measured using the automatic gas adsorption apparatus Belsorp 28SA [24]. A catalyst sample was placed in an adsorption vessel and activated in hydrogen flow at 673 K for 3 h followed by evacuation at 673 K for 3 h, and then cooled to an adsorption temperature of 373 K and held at that temperature for 3 h. 6.67 kPa of hydrogen was then introduced into the adsorption system, and the pressure change was monitored with time to calculate the hydrogen uptake.

2.4. Catalytic reaction of *n*-butane

Isomerization of *n*-butane was carried out in a closed recirculation batch reactor at 573 K [2]. 0.3 g of catalyst was activated with circulating of 40 kPa of hydrogen at 673 K for 3 h followed by evacuation at 673 K for 3 h. 46.67 kPa of mixture containing hydrogen and *n*-butane with the ratio 6:1 was allowed to react at 573 K. In order to evaluate the role of hydrogen, the nitrogen gas was also used as a carrier gas. The products were analyzed with an on-line 6090N Agilent Gas Chromatograph equipped with VZ-7 packed column and FID detector. No by-product was observed in this reaction.

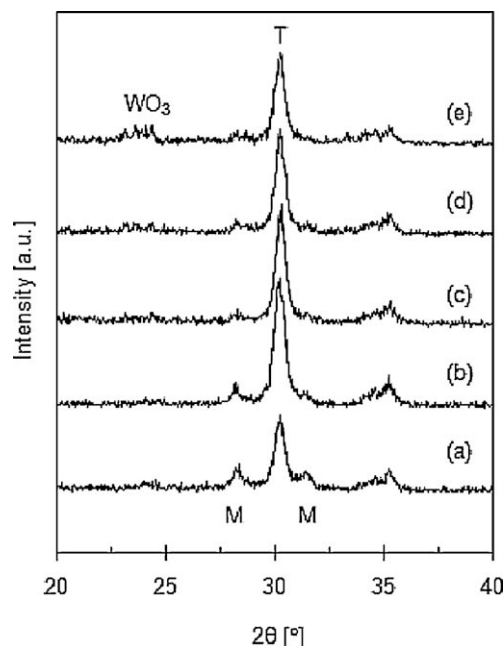


Fig. 1. Powder X-ray diffraction pattern for WZ catalysts containing different amount of WO_3 : (a) 5WZ, (b) 10WZ, (c) 13WZ, (d) 15WZ, (e) 20WZ catalysts.

The total conversion of *n*-butane ($X_{n\text{-butane}}$) was calculated according to Eq. (5).

$$X_{n\text{-butane}} = \frac{[C]_{\text{isobutane}}}{[C]_{\text{isobutane}} + [C]_{\text{residual } n\text{-butane}}} \quad (5)$$

where $[C]$ is a mol number for particular compound which is calculating based on the Scott hydrocarbon calibration standard gas (Air Liquide America Specialty Gases LLC).

3. Results and discussion

Fig. 1 shows the XRD patterns for WZ catalysts. The peak at $2\theta = 30.2^\circ$ was assigned to the tetragonal phase of ZrO_2 and the peaks at $2\theta = 28.2^\circ$ and 31.8° to the monoclinic phase of ZrO_2 . The peak ascribed to the tetragonal phase of ZrO_2 was predominant and small peaks of the monoclinic phase of ZrO_2 were observed for all WZ catalysts. Weak and broad peaks ascribed to the crystal structure of bulk WO_3 at about $2\theta = 23\text{--}25^\circ$ were observed for catalysts with 15 and 20 wt% WO_3 loading. This result may indicate the existence of free tungstate anions on the surface of the catalyst which formed bulk crystalline WO_3 during calcination at 1093 K. However, the WO_3 -free ZrO_2 consisted almost completely of the monoclinic phase of ZrO_2 and the phase of ZrO_2 did not change much if crystalline ZrO_2 was used as the support in the preparation of the catalyst. Increasing the WO_3 loading led to a continuous decrease in peaks ascribed to monoclinic phase of ZrO_2 and an increase in the peak ascribed to the tetragonal phase of ZrO_2 . The change in the phase of ZrO_2 was almost not observed for high loading of WO_3 . Stabilization of the tetragonal phase of ZrO_2 and delaying or inhibiting the sintering of ZrO_2 crystallites are caused by the anchoring tungstate anion in $\text{Zr}(\text{OH})_4$ hydroxyl groups. The stabilization effect of tungsten oxo-species in the tetragonal phase of ZrO_2 is consistent with previous reports [25–29]. Scheithauer et al. reported that the monoclinic phase of ZrO_2 dominated at 7.5 wt% WO_3 and was lower when the catalyst was calcined at 1098 K. An increase in WO_3 loading up to 19 wt% WO_3 increased the fraction of the tetragonal phase of ZrO_2 . This result indicates that minimum WO_3 loading is required to inhibit the formation of the monoclinic phase of ZrO_2 [25]. On the contrary, Vu et al. reported that

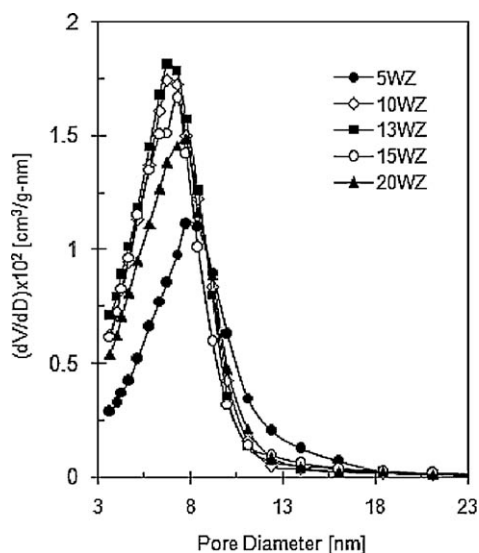


Fig. 2. Pore size distribution for WZ catalysts containing different amount of WO_3 .

tungsten loading did not affect the XRD pattern of a ZrO_2 support due to the stabilization of ZrO_2 already achieved by the incorporation silicon in the preparation [30]. In addition, Vaudagna et al. reported that bulk crystalline WO_3 was formed by calcination of the catalysts at 1103 K regardless of the degree of WO_3 loading [29], while Scheithauer et al. concluded that crystalline WO_3 was formed only for 19 wt% WO_3 loading on ZrO_2 with calcination temperatures of 1023 K and above [25].

The crystal phase, specific surface area, total pore volume, WO_3 surface density and WO_3 coverage are summarized in Table 1. With increasing WO_3 loading, the ratio of the monoclinic to tetragonal phases of ZrO_2 decreased and, in contrast, the surface density and coverage of WO_3 continuously increased. The 13WZ catalyst, which provided the maximum specific surface area, corresponded to ca. $5.9 \text{WO}_3/\text{nm}^2$ as the surface concentration of WO_3 , which is near the theoretical monolayer-dispersed limit of WO_3 in this experiment. The specific surface area and total pore volume of ZrO_2 obtained by calcination of $\text{Zr}(\text{OH})_4$ at 1093 K were $25 \text{ m}^2/\text{g}$ and 0.030 ml/g , respectively. These values are lower than those of ZrO_2 -supported WO_3 catalysts, indicating the inhibition effect of WO_3 species in the sintering of ZrO_2 supports. The specific surface area and total pore volume of the catalysts increased with WO_3 loading and reached a maximum value at 13 wt% WO_3 loading. The further addition of WO_3 slightly decreased both surface area and total pore volume. These decreases were not caused by ZrO_2 phase collapse, but most probably occurred after WO_3 coverage reached the theoretical monolayer limit, and the excess amorphous or crystalline WO_3 narrowed or plugged the pores of the catalyst, leading to a decrease in the specific surface area and pore volume after reaching a maximum. The dV/dD function for all WZ catalysts presented sharp peaks centered at 6–8 nm (Fig. 2). The peak at 7.8 nm for the 5WZ catalyst intensified and shifted to a smaller pore diameter with increasing WO_3 loading, up to 13 wt%, indicating the penetration of WO_3 into large pores to form pores of relatively small diameter. The further addition of WO_3 lowered the small pore diameter intensities due to the plugging of small diameter pores.

Figs. 3 and 4 show the IR spectra in the O–H and W=O stretching regions of the activated and pyridine adsorbed WZ catalysts. The catalysts were activated at 673 K, followed by the adsorption of pyridine at 423 K and outgassing at 623 K. The activated 5WZ catalyst showed broad bands centered at 3738 and 3650 cm^{-1} , inferring the existence of several hydroxyl stretching bands with different acidic centers and strength (Fig. 3). These bands were

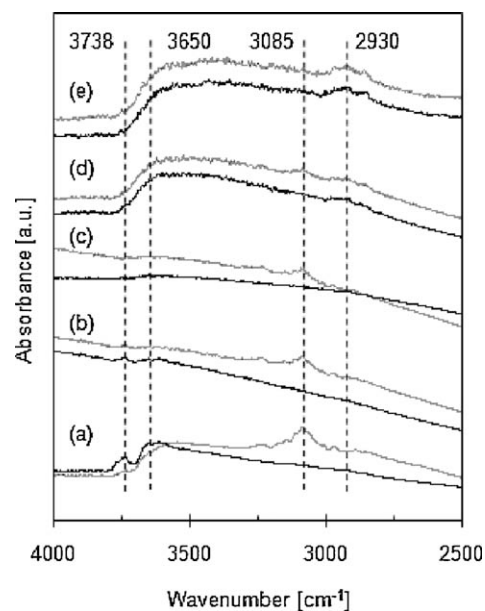


Fig. 3. IR spectra in the hydroxyl stretching region for activated and pyridine adsorbed WZ catalysts containing different amount of WO_3 : (a) 5WZ, (b) 10WZ, (c) 13WZ, (d) 15WZ, (e) 20WZ catalysts.

assigned to bibriged and tribridged hydroxyl groups, indicating the presence of both the tetragonal and monoclinic phases of zirconia on the catalyst [20,31]. Both bands eroded continuously with increased WO_3 loading, and the intensity of the hydroxyl stretching bands totally disappeared at 13 wt% WO_3 loading, indicating that both bibriged and tribridged hydroxyl groups on the surface were covered by tungstate anions. Further loading of WO_3 led to new broad bands at $3500\text{--}3700$ and $2800\text{--}3000 \text{ cm}^{-1}$, corresponding to the preferential formation of $\text{Zr}\text{--O}\text{--W}$ and $\text{W}\text{--O}\text{--W}$ terminations of crystallite planes, respectively. In addition, two absorbance bands were observed in the W=O stretching regions at $1025\text{--}2010 \text{ cm}^{-1}$ for all WZ catalysts (Fig. 4). The main band at a higher wavenumber was relatively sharp and stronger, and

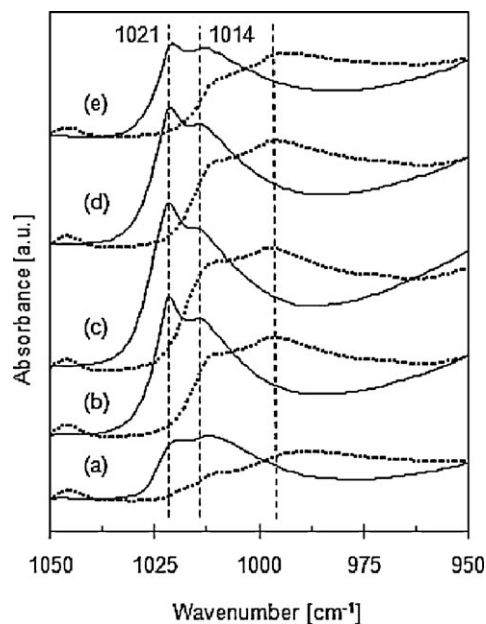


Fig. 4. IR spectra in the W=O stretching region for activated and pyridine adsorbed WZ catalysts containing different amount of WO_3 : (a) 5WZ, (b) 10WZ, (c) 13WZ, (d) 15WZ, (e) 20WZ catalysts.

Table 1
Composition and physico-chemical properties of tungstated zirconia catalysts.

Catalyst	WO ₃ content (wt%)	M/T ^a (%/%)	Surface area (m ² /g)	Pore volume (ml/g)	Surface density (WO ₃ /nm ²)	WO ₃ coverage (%)
5WZ	5	38/62	33	0.068	3.9	61
10WZ	10	19/81	46	0.086	5.6	87
13WZ	13	11/89	57	0.098	5.9	92
15WZ	15	5/95	49	0.089	8.0	124
20WZ	20	5/95	44	0.070	11.8	171

^a Monoclinic/tetragonal phase of ZrO₂.

the shoulder band at a lower wavenumber was much weaker and broader. Increased WO₃ loading did not change the position of the band at 1021 cm⁻¹, whereas the band at 1014 cm⁻¹ was observed only for the 13WZ catalyst. The peak at 1014 cm⁻¹ shifted slightly to a lower wavenumber for the 5WZ, 10WZ, 15WZ and 20WZ catalysts. Based on our previous assignment, the bands at 1021 and 1014 cm⁻¹ for 13WZ were assigned to the stretching of W=O connected to coordinative unsaturated (cus) Zr⁴⁺ through O and to the other W through O, respectively [32]. No dioxo (O=W=O) tungsten oxide species were present in any of the catalysts, as seen by the absence of IR bands for symmetric and antisymmetric stretching modes of the O=W=O bond with different relative intensities and wavenumbers (30–50 cm⁻¹ difference). The spectra in the O–H and W=O stretching regions were essentially the same as those reported by Naito et al. [15] and Scheithauer et al. [14,25] for dehydrated WZ catalysts. Naito et al. reported a band assigned to the hydroxyl group observed at 3676 cm⁻¹ for both ZrO₂ and WZ catalysts. Scheithauer et al. reported the O–H stretching region in the range of 3777–3741 cm⁻¹, although the band position of the hydroxyl groups varied in the catalysts containing different amounts of WO₃ loading and following calcination at different temperatures. In addition to the hydroxyl groups, Scheithauer et al. concluded, together with the Raman spectra data, that the two bands at 1024 and 1005 cm⁻¹ are characteristic of two independent W=O species. Similar to the hydroxyl groups, the W=O band positions varied in the catalysts containing different amounts of WO₃ loading.

Both O–H and W=O bands for WZ catalysts in this experiments were affected by pyridine adsorption due to the inductive effects by pyridine coordinated to cus Zr⁴⁺ sites in the vicinity of WO_x. Particularly, W=O groups connected to cus Zr⁴⁺ should be affected more extensively than the other types of W=O groups. Adsorption of pyridine at 423 K followed by outgassing at 623 K shifted the W=O bands to a lower frequency and changed the intensity of the bands. Adsorption bands at 1021 and 1014 cm⁻¹ for all WZ catalysts shifted to 1014 and 995 cm⁻¹, respectively (Fig. 4). In addition to the shift in the band positions, the intensity of the band at 1021 cm⁻¹ decreased more extensively compared to the band at 1014 cm⁻¹, indicating that the peak at 1021 cm⁻¹ is the W=O band connected to cus Zr⁴⁺ sites through an O atom. In addition to the changes in the W=O absorbance bands, the adsorption of pyridine on the 5WZ catalyst eroded the hydroxyl stretching bands centered at 3738 and 3650 cm⁻¹ and the new band centered at 3085 cm⁻¹, which may be related to pyridine coordinated to cus Zr⁴⁺ sites (Fig. 3). The bands at about 3085 cm⁻¹ eroded with increasing WO₃ loading and diminished at higher WO₃ loading. However, 15WZ and 20WZ formed new weak and broad bands centered at 2930 and 2860 cm⁻¹; these bands were unaffected by the adsorption of pyridine, indicating the existence of bulk crystalline WO₃ on the catalyst surface. This result is in good agreement with the XRD results in which crystalline WO₃ was observed only in the 15WZ and 20WZ catalysts.

Acid site distribution and strength for WZ catalysts were studied by NH₃-TPD and pyridine adsorbed IR spectroscopy (Fig. 5). The NH₃-TPD results show that ammonia desorbed in one large envelope centered at 453 K for all WZ catalysts (Fig. 5A). The shoulder band which emerged when the catalysts were heated to 1200 K

reveals that the surface acid strength was widely distributed on the catalysts. Gaussian deconvolution of NH₃-TPD spectrum for 13WZ indicated the existence of NH₃ desorption peaks centered at 440, 470, 560, 665 and 720 K which inferring that there are several type of acidic centers with different strengths of acidity (Fig. 5C). No ammonia was desorbed at 900 K and above. The NH₃-TPD curves also indicated that the amount of adsorbed ammonia increased with increasing WO₃ loading and reached a maximum at 13 wt% WO₃ loading. This result reveals that the total number of acid sites was determined by the WO₃ coverage in which the maximum acidity of catalysts was obtained when the ZrO₂ catalyst was covered by monolayer-dispersed WO₃. In fact, a further increase in WO₃ loading decreased the intensity of the peaks centered at 453 K. Fig. 5B shows the IR spectra of pyridine adsorbed on WZ

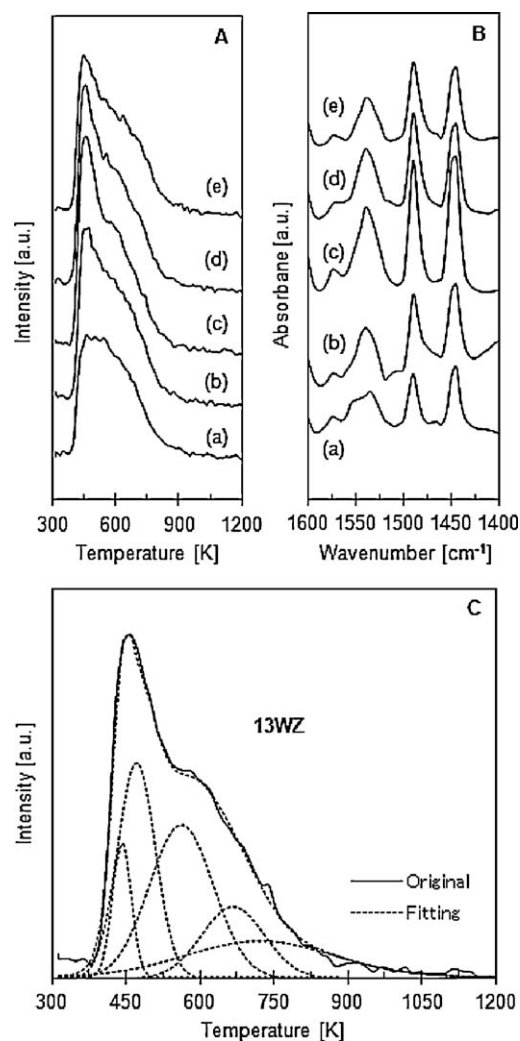


Fig. 5. (A) NH₃-TPD and (B) pyridine adsorption plots for WZ catalysts containing different amount of WO₃: (a) 5WZ, (b) 10WZ, (c) 13WZ, (d) 15WZ, (e) 20WZ catalysts. (C) NH₃-TPD spectrum and Gaussian deconvolution peaks for 13WZ catalyst.

catalysts. The IR bands at 1540 and 1450 cm^{-1} assigned to pyridinium ions adsorbed on protonic acid sites and pyridine coordinated to Lewis acid sites appeared for all WZ catalysts, respectively. As WO_3 loading increased, the bands at 1540 and 1450 cm^{-1} continuously intensified and reached a maximum at 13 wt% WO_3 loading. A further increase in WO_3 loading decreased the intensity of both peaks at 1540 and 1450 cm^{-1} . The decrease in the intensity was much greater on Lewis acid sites than on Brønsted acid sites for 15 and 20 wt% WO_3 loaded catalysts due to the presence of WO_3 coverage exceeding the theoretical monolayer-dispersion limit on the surface of ZrO_2 , which lowered the accessibility of Lewis acid sites to pyridine. This result resembles the NH_3 -TPD result in which the acidity of the catalyst was determined by the WO_3 coverage. Studies on the acidity of WZ have been reported by Sun et al. [33] and Naito et al. [15] using ammonia TPD and IR spectroscopy. Based on NH_3 -TPD, Sun et al. reported that WZ catalysts containing 3.8–34.1 wt% WO_3 possess two kinds of acidic centers from which ammonia desorbs at 400 and 500 K. However, Naito et al. reported that the introduction of WO_3 on ZrO_2 developed new bands assigned to the interaction of hydroxyl groups with ammonia at 3344, 3262 and 3180 cm^{-1} . Other peaks corresponding to the ammonia species adsorbed on WO_3 -loaded ZrO_2 were observed at 1608, 1433 and 1262 cm^{-1} . In contrast, different results of pyridine adsorbed IR were found by Naito et al., in which they reported that an increase in WO_3 loading continuously decreased the Lewis acid sites, while the Brønsted acid sites showed a maximum at 6 W atoms/ nm^2 catalyst. Both acidic sites totally diminished for the catalyst containing 17.3 W atoms/ nm^2 . This conclusion is rather similar to the CO adsorption results reported by Scheithauer et al., in which the Lewis acid sites were not observed in all WZ samples with WO_3 loading beyond the saturation value as all the Zr^{4+} on the surface was covered by WO_3 [14,25]. Our research group has also reported on a pyridine adsorbed IR study of WZ and Pt-loaded WZ catalysts [9]. For both WZ and Pt/WZ, all the protonic acid sites were strong; pyridine molecules remained at the protonic acid sites after outgassing at 673 K. In addition to strong Lewis acid sites, there existed a number of weak Lewis acid sites from which the pyridine molecules were desorbed in the temperature range of 423–673 K. The ratio of Lewis acid sites to protonic acid sites increased with an increase in the treatment temperature for both WZ and Pt/WZ. The presence of Pt did not considerably change the permanent Lewis and Brønsted acid sites; however, it markedly enhanced the formation rate of protonic acid sites from molecular hydrogen through a hydrogen spillover mechanism.

Fig. 6 shows the variation in isothermal hydrogen adsorption as a function of time at 373 K for activated WZ catalysts. Similar features of hydrogen adsorption were observed for WZ catalysts with different amounts of WO_3 loading. For the initial few minutes, fast adsorption occurred and the hydrogen uptake achieved near equilibrium within 10 h. At equilibrium, the hydrogen uptake increased with increasing WO_3 loading and reached a maximum at 13 wt% with a hydrogen uptake capacity of 6.09×10^{18} H atoms/ m^2 cat. The high concentration of hydrogen uptake on 13WZ may be related to the mechanism and structure of H^+ bounded to O atom on WZ. We have proposed that H^+ from molecular hydrogen bounds to three O atoms, two O atoms bridging Zr and W, and one O atom in the $\text{W}=\text{O}$ of which W is connected to Zr through O. The H^+ may be mobile among the three O atoms [32]. Therefore, the maximum capacity of WZ to adsorb H^+ is at least similar to the number of W atom connected to Zr through O. Beyond the monolayer-dispersed WO_3 , increasing of the number of W did not necessarily increase the capacity of WZ to uptake H^+ . In fact, the hydrogen uptake capacity decreased with the addition of 15 and 20 wt% WO_3 . This decrease may have been caused by a reduction in Lewis acid sites as the WO_3 on the catalyst surface had exceeded the theoretical limit of monolayer-dispersed WO_3 . We have reported studies of hydrogen

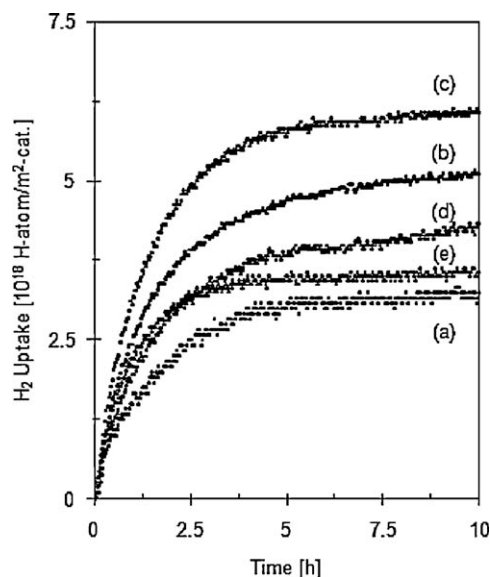


Fig. 6. Variations of hydrogen uptake as a function of time for WZ catalysts containing different amount of WO_3 : (a) 5WZ, (b) 10WZ, (c) 13WZ, (d) 15WZ, (e) 20WZ catalysts.

adsorption on WZ, MZ and Pt/ MoO_3 catalysts evidenced by IR spectroscopy and quantitative hydrogen uptake measurements [24,34–36]. The hydrogen adsorption on those catalysts was characterized by the dissociation of molecular hydrogen into hydrogen atoms, spillover of hydrogen atoms, surface diffusion of spillover hydrogen atoms and the formation of H^+ or H_xMoO_3 . The presence of specific active sites and strong Lewis acid sites are required for hydrogen adsorption in which specific active sites such as Pt, acidic sites or reduced WO_3 or MoO_3 facilitate the dissociative adsorption of molecular hydrogen and Lewis acid sites stabilize a proton by trapping an electron from a hydrogen atom. Therefore, stronger Lewis acid sites form a larger number of protonic acid sites from molecular hydrogen. The hydrogen adsorption kinetic behavior is different between WZ, MZ and Pt/ MoO_3 catalysts. The rate-controlling step of hydrogen adsorption is surface diffusion of spilt-over hydrogen atoms for all WZ, MZ and Pt/ MoO_3 catalysts with apparent activation energies of 25.9, 62.8 and 83.1 kJ/mol, respectively [34–36]. The difference in the apparent activation energies may be caused by differences in the acidity of the catalyst, which leads to differences in hydrogen-surfaces interaction and/or the ease of surface diffusion of hydrogen atoms. Other difference among WZ, MZ and Pt/ MoO_3 catalysts is the necessity for specific active sites to facilitate the dissociative adsorption of hydrogen. Pt is required for MoO_3 catalysts, but hydrogen uptake is considerable for Pt-free WZ and MZ. It seems that acidic sites on the catalysts act as active sites to dissociate hydrogen molecules into hydrogen atoms [34]. Barton et al. [18] have reported on the relationship between tungsten loading and hydrogen uptake capacity of tungstated zirconia catalysts. They concluded that hydrogen uptake increases with tungsten loading due to the stabilization of hydrogen by polytungstate and crystalline WO_3 species on the surface ZrO_2 . However, WO_x species, which are present below the theoretical monolayer coverage, cannot accommodate hydrogen due to the inability of WO_x species to delocalize the negative charge required to stabilize the $\text{H}^{\alpha+}$ concentration.

The hydrogen uptake capacity of WZ catalysts was confirmed by the formation of protonic acid sites from molecular hydrogen as evidenced by IR spectroscopy. Fig. 7 shows the features of the formation of protonic acid sites from molecular hydrogen for 5WZ, 13WZ and 20WZ. The results for 10WZ and 15WZ are not shown here. A similar trend was observed for all catalysts in which the

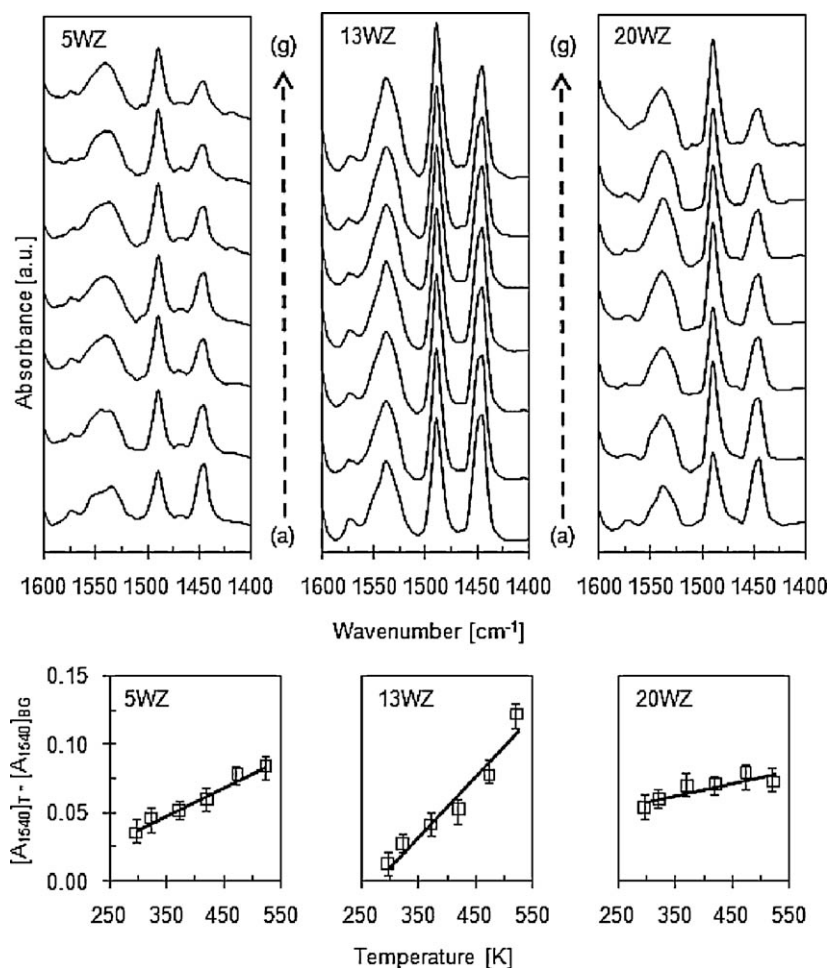


Fig. 7. IR spectra of pyridine adsorbed on WZ catalysts (above) and temperature dependencies of formation of protonic acid sites from molecular hydrogen (bottom). Spectral changes when pyridine-preadsorbed sample was heated in hydrogen at (b) room temperature, (c) 323 K, (d) 373 K, (e) 423 K, (f) 473 and (g) 523 K. (a) Before exposure to hydrogen.

heating of pyridine preadsorbed catalysts in the presence of hydrogen in gas phase increased the intensity of the band at 1540 cm⁻¹ assigned to the protonic acid sites and simultaneously decreased the intensity of the band at 1450 cm⁻¹ assigned to the Lewis acid sites. Two absorbance bands at 1460 and 1475 cm⁻¹ assigned to adsorbed piperidine were not observed in the heating of WZ up to 523 K indicating the hydrogenation of pyridine did not take place. The changes of absorbance bands at 1450 and 1540 cm⁻¹ reveals that the protonic acid sites were formed from molecular hydrogen through a hydrogen spillover mechanism facilitated Lewis acidic sites as electron acceptors. Based on our previous assignment, it is plausible that the H⁺ is loosely bound to three O atoms, i.e. two O atoms bridging Zr and W, and one O atom in W=O of which W is connected to Zr through O. The H⁺ may be mobile among the three O atoms [32]. The effect of WO₃ loading in the formation of protonic acid sites is clearly seen if the number of protonic acid sites formed is plotted against the heating temperature. Although the results for the 10WZ and 15WZ catalysts are not shown here, the steepest incline of the plot of $[A_{1540}]_T - [A_{1540}]_{BG}$ versus T was observed for the 13WZ catalyst, indicating the highest ability and capacity to form and to take up protonic acid sites from molecular hydrogen. This result agrees with the acidity of the catalysts in which the 13WZ catalyst possessed the highest acidity of the catalysts, particularly Lewis acid sites. This also confirmed that the acidity of the catalyst plays an important role in hydrogen uptake or the formation of protonic acid sites over WZ catalysts.

The isomerization of *n*-butane was carried out at 573 K in a closed recirculation batch reactor with a mixture of H₂ (40 kPa) or N₂ (40 kPa) and *n*-butane (6.67 kPa). In the presence of hydrogen gas, the product consisted of only isobutane and residual *n*-butane. It is interesting to note that neither lower nor higher linear alkanes were observed, indicating that dimerization, hydrogenolysis or cracking did not take place. The different result was observed when the isomerization was done in a pulse or continuous flow reactor in which the isomerization took place either in the presence or absence of molecular hydrogen [10,23]. The differences in the reaction system and activation technique may be resulted in the different observation. The time dependencies and the effect of WO₃ loading in the yield of the reaction are shown in Fig. 8A and B, respectively. In the presence of H₂, the activity of WZ in *n*-butane isomerization was strongly determined by the amount of WO₃ loading. Fig. 8A shows that increasing WO₃ loading improved the yield of isobutane and reached a maximum for 13WZ, which may have been due to the highest formation rate of protonic acid sites or hydrogen uptake capacity. In addition, the 13WZ catalyst possessed the highest number of strong Lewis acid sites corresponding to the tetragonal phase of ZrO₂ in which this type of Lewis acid site may play an important role in the formation of active protonic acid sites for isomerization [23]. This activity was not observed for the WO₃-free ZrO₂ catalyst (data not shown), which may have been due to the absence of strong Lewis acid sites corresponding to the tetragonal phase of zirconia [10,37]. In general, high activity was observed

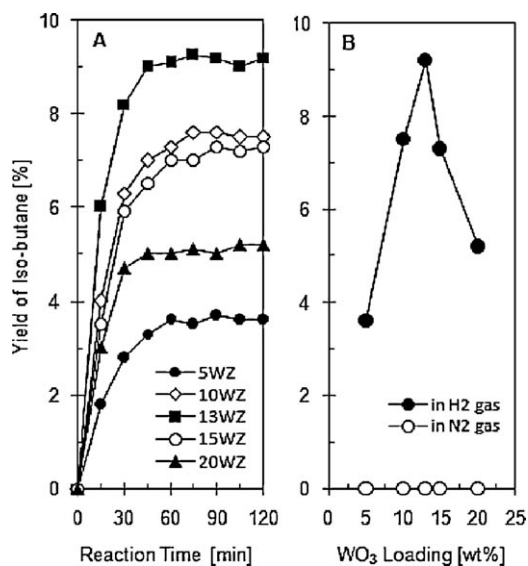


Fig. 8. Time dependences of the yield of isobutane for WZ catalysts containing different amount of WO₃: (a) 5WZ, (b) 10WZ, (c) 13WZ, (d) 15WZ, (e) 20WZ catalysts. (B) *n*-Butane isomerization at 573 K as a function of WO₃ loading (data was taken at $t = 120$ min in (A)).

in the initial 30 min of the reaction with no-induction period was observed in this WZ which may be due to reaction system and/or the activation method in this experiment (H₂-circulating at 673 K for 3 h, followed by outgassing at 673 K for 3 h) [38]. The activity of the catalysts decreased gradually and totally lost their activity within 120 min for all WZ catalysts. The rapid deactivation may have been caused by the poor ability of WZ catalysts to form or to maintain active protonic acid sites and/or to remove coke deposits on the catalyst surface due to the absence of strong specific active sites like Pt metal for dissociative adsorption of molecular hydrogen. Indeed, none of the WZ catalysts showed any activity when hydrogen gas was changed to nitrogen gas (Fig. 8B). Thus, we suggest that the introduction of specific active sites for dissociative adsorption of molecular hydrogen, such as Pt or Pd, is necessary in order to improve and to maintain the activity and stability of WZ catalysts.

Fig. 9 shows the plots of the dependence of activity of WZ upon the hydrogen uptake capacity and WO₃ loading. The results showed a direct correlation between hydrogen uptake and the activity of WZ in *n*-butane isomerization at 573 K. The yield ratio of isobutane to hydrogen uptake capacity did not change much for any of the WZ catalysts, indicating that the activity of WZ catalysts is clearly correlated with the number of hydrogen uptake on WZ catalysts. While, the dependence of activity of WZ on the number of W atom loading was only observed at and below monolayer-dispersed WO₃. Beyond the monolayer coverage, the activity of WZ decreased markedly due to the formation of multilayer-dispersed WO₃ on the surface ZrO₂ which hindering the accessibility of all W atoms to the reactant.

The activity of WZ catalysts has been explored widely in the last two decades. Hino and Arata reported that the activity of WZ is not high enough to isomerize *n*-butane compared to SZ catalysts [26]. Therefore, they mechanically mixed WZ with Pt-loaded metal oxides to enhance *n*-butane isomerization. The results showed that the effect of mixing was specific only to Pt/ZrO₂. Mixing WZ with Pt/TiO₂, Pt/Al₂O₃, Pt/Fe₂O₃ or Pt/SnO₂ did not show any activity in *n*-butane isomerization. They concluded that only Pt on ZrO₂ formed cationic Pt, which was active in the isomerization of *n*-butane. Rossi et al. reported the effect calcination temperature and the role of hydrogen in the gas phase [39]. They concluded that

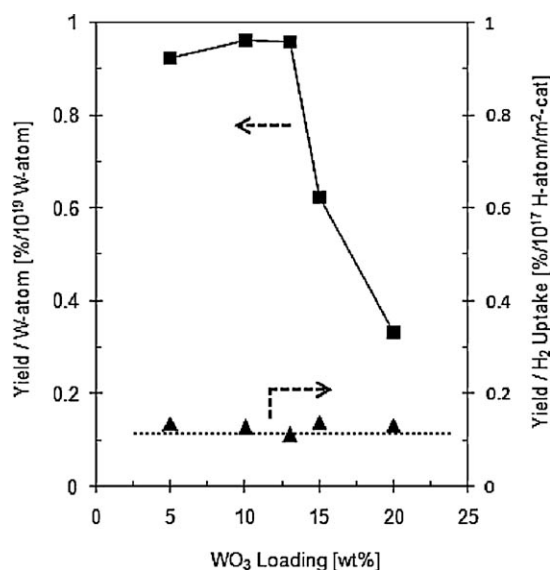


Fig. 9. Hydrogen uptake and W atoms loading dependences of the yield of isobutane for WZ catalysts containing different amount of WO₃. Isomerization was carried out at 573 K under the presence of hydrogen gas.

a higher calcination temperature is required to obtain high activity of WZ catalysts. In addition, they stated that hydrogen gas has a role in the removal of coke by inhibiting the dehydrogenation process and in shortening the induction period, indicating the formation of active hydroxyl groups from hydrogen in the gas phase. Naito et al. reported the effect of WO₃ loading on *n*-butane isomerization in which the maximum activity was obtained at 6.4 W atoms/nm² catalyst; further W loading diminished the activity of the catalyst. They also concluded that the presence of Brønsted acid sites on the monolayer was responsible for high activity in *n*-butane isomerization.

The activity of WZ was also observed in *n*-pentane and xylene isomerization. Santiesteban et al. concluded that the activity of WZ in *n*-pentane isomerization passed through a maximum as W loading increased [28]. The activity reached a maximum at approximately 16 wt% W loading on ZrO₂; this loading represents about twofold the monolayer coverage of the WO₄²⁻ species. In addition, they also concluded that the activity of WZ was strongly dependent on the reducibility of tungsten oxospecies on ZrO₂, i.e. WZ catalysts containing higher tungsten oxospecies are relatively active due to the ease of reduction compared to lower tungsten oxospecies catalysts. Scheithauer et al. reported that an increase in the tungsten loading continuously increased the number of Brønsted acid sites such that the activity of the catalyst for *n*-pentane isomerization corresponded to the strength and number of permanent Brønsted acid sites [14]. However, the Lewis acid sites reached a maximum and started to decline as the loading reached saturation. The role of hydrogen gas was clarified with *o*-xylene isomerization in which hydrogen gas played an important role in promotion of the reaction rate and a decrease in the catalyst deactivation rate by maintaining the Brønsted acid site concentration and reversing the xylene dehydrogenation steps [40].

4. Conclusion

The introduction of WO₃ on ZrO₂ continuously increased the tetragonal phase of ZrO₂ as well as WO₃ surface density and coverage. The specific surface area and total pore volume passed through a maximum near the theoretical monolayer-dispersed limit of WO₃ at 13 wt% WO₃ loading; this amount of WO₃ corresponds to 5.9 WO₃/nm². The IR results indicate that WO₃ interacted with

bi-bridged and tri-bridged hydroxyl groups at 3738 and 3650 cm^{-1} . These absorbance bands totally disappeared at 13 wt% WO_3 loading, indicating that the hydroxyl groups had been fully covered by WO_3 . A new absorbance band appeared centered at 2930 cm^{-1} , indicating the development of bulk crystalline WO_3 for WO_3 coverage exceeding the theoretical monolayer-dispersion limit. In addition to the OH stretching bands, two W=O stretching bands were observed at about 1021 and 1014 cm^{-1} for all WZ catalysts, confirming the existence of W=O connected to cus Zr^{4+} through O and to the other W through O, respectively. Pyridine adsorbed IR and NH_3 -TPD revealed that the addition of WO_3 clearly modifies the nature and concentration of the acidic sites. The highest acidity was observed for 13 wt% WO_3 loading; a further increase in WO_3 loading decreased both Lewis and Brønsted acid sites. The interaction of hydrogen in the gas phase with the catalyst surface was observed by hydrogen adsorption isotherms and hydrogen adsorption on preadsorbed pyridine IR spectroscopy. The maximum hydrogen uptake capacity and highest formation rate of protonic acid sites were observed for 13 wt% WO_3 loading of the ZrO_2 catalyst. These results show a direct correlation with the activity of WZ in *n*-butane isomerization at 573 K in which 13 wt% WO_3 loading on ZrO_2 yielded the highest amount of isobutane in the presence of hydrogen in the gas phase. The presence of strong Lewis acid sites corresponds to tetragonal phase of ZrO_2 enhanced the formation of active protonic acid sites for *n*-butane isomerization. In fact, no isomerization activity was observed in the absence of hydrogen. Thus, it is suggested that the presence of permanent Brønsted acid sites cannot be directly associated with the activity of WO_3 loaded ZrO_2 catalysts.

Acknowledgements

This work was supported by The Ministry of Higher Education, Malaysia through the Fundamental Research Grant Scheme No. 78670. We also thank the Hitachi Scholarship Foundation for the Gas Chromatograph Instruments Grant.

References

- [1] K. Ebitani, J. Konishi, H. Hattori, *J. Catal.* 130 (1991) 257–267.
- [2] S. Triwahyono, T. Yamada, H. Hattori, *Catal. Lett.* 85 (2003) 109–115.
- [3] P. Afanasiev, *Mater. Chem. Phys.* 47 (1997) 231–238.
- [4] B. Samaranch, P.R. Piscina, G. Clet, M. Houalla, N. Homs, *Chem. Mater.* 18 (2006) 1581–1586.
- [5] K. Tomishige, A. Okabe, K. Fujimoto, *Appl. Catal. A: Gen.* 194 (2000) 383–393.
- [6] T.-X. Cheng, H. Kabashima, H. Hattori, *React. Kinet. Catal. Lett.* 69 (2000) 201–207.
- [7] C.R. Vera, C.L. Pieck, K. Shimizu, C.A. Querini, J.M. Parera, *J. Catal.* 187 (1999) 39–49.
- [8] H. Hattori, T. Shishido, *Catal. Surv. Jpn.* 1 (1997) 205–213.
- [9] S. Triwahyono, T. Yamada, H. Hattori, *Appl. Catal. A: Gen.* 242 (2003) 101–109.
- [10] N.N. Ruslan, N.A. Fadzilliah, A.H. Karim, A.A. Jalil, S. Triwahyono, *Appl. Catal. A: Gen.* 406 (2011) 102–112.
- [11] S. Triwahyono, A.A. Jalil, M. Musthofa, *Appl. Catal. A: Gen.* 372 (2010) 90–93.
- [12] M.A.A. Aziz, N.H.N. Kamarudin, H.D. Setiabudi, H. Hamdan, A.A. Jalil, S. Triwahyono, *J. Nat. Gas Chem.* 21 (2012) 29–36.
- [13] H.D. Setiabudi, S. Triwahyono, A.A. Jalil, N.H.N. Kamarudin, M.A.A. Aziz, *J. Nat. Gas Chem.* 20 (2011) 477–482.
- [14] M. Scheithauer, T.-K. Cheung, R.E. Jentoft, R.K. Grasselli, B.C. Gates, H. Knozinger, *J. Catal.* 180 (1998) 1–13.
- [15] N. Naito, N. Katada, M. Niwa, *J. Phys. Chem. B* 103 (1999) 7206–7213.
- [16] V. Lebarbier, G. Clet, M. Houalla, *J. Phys. Chem. B* 110 (2006) 13905–13911.
- [17] N. Soultanidis, W. Zhou, A.C. Psarras, A.J. Gonzalez, E.F. Iliopoulou, C.J. Kiely, I.E. Wachs, M.S. Wong, *J. Am. Chem. Soc.* 132 (2010) 13462–13471.
- [18] D.G. Barton, S.L. Soled, G.D. Meitzner, G.A. Fuentes, E. Iglesia, *J. Catal.* 181 (1999) 57–72.
- [19] J.C. Vartuli, J.G. Santiesteban, P. Traverso, N. Cardona-Martinez, C.D. Chang, S.A. Stevenson, *J. Catal.* 187 (1999) 131–138.
- [20] S. Triwahyono, Z.A. Abdullah, A. Jalil, *J. Nat. Gas Chem.* 15 (2006) 247–252.
- [21] H. Toraya, S. Yoshimura, S. Somyia, *J. Am. Ceram. Soc.* 67 (1984) 119–121.
- [22] S. Triwahyono, A.A. Jalil, R.R. Mukti, M. Musthofa, N.A.M. Razali, M.A.A. Aziz, *Appl. Catal. A: Gen.* 407 (2011) 91–99.
- [23] H.D. Setiabudi, A.A. Jalil, S. Triwahyono, N.H.N. Kamarudin, R.R. Mukti, *Appl. Catal. A: Gen.* 417–418 (2012) 190–199.
- [24] S. Triwahyono, A.A. Jalil, H. Hattori, *J. Nat. Gas Chem.* 16 (2007) 252–257.
- [25] M. Scheithauer, R.K. Grasselli, H. Knozinger, *Langmuir* 14 (1998) 3019–3029.
- [26] M. Hino, K. Arata, *Appl. Catal. A: Gen.* 169 (1998) 151–155.
- [27] C. Mortera, G. Cerrato, V. Bolis, C. Lamberti, L. Ferroni, L. Montanaro, *J. Chem. Soc. Faraday Trans.* 91 (1995) 113–123.
- [28] J.G. Santiesteban, J.C. Vartuli, S.H. Han, R.D. Bastian, C.D. Chang, *J. Catal.* 168 (1997) 431–441.
- [29] S.R. Vaudagna, S.A. Canavese, R.A. Comelli, N.S. Figoli, *Appl. Catal. A: Gen.* 168 (1998) 93–111.
- [30] T.N. Vu, J. van Gestel, J.P. Gilson, C. Collet, *J. Catal.* 231 (2005) 453–467.
- [31] K.T. Jung, A.T. Bell, *J. Mol. Catal. A: Chem.* 163 (2000) 27–42.
- [32] S. Triwahyono, T. Yamada, H. Hattori, *Appl. Catal. A: Gen.* 250 (2003) 75–81.
- [33] W.-D. Sun, Z.-B. Zhao, C. Guo, X.-K. Ye, Y. Wu, *Ind. Eng. Chem. Res.* 39 (2000) 3717–3725.
- [34] S. Triwahyono, T. Yamada, H. Hattori, *Appl. Catal. A: Gen.* 250 (2003) 65–73.
- [35] N.N. Ruslan, S. Triwahyono, A.A. Jalil, S.N. Timmiati, N.H.R. Annuar, *Appl. Catal. A: Gen.* 413–414 (2012) 176–182.
- [36] S. Triwahyono, A.A. Jalil, S.N. Timmiati, N.N. Ruslan, H. Hattori, *Appl. Catal. A: Gen.* 372 (2010) 103–107.
- [37] C.R. Vera, C.L. Pieck, K. Shimizu, J.M. Parera, *Appl. Catal. A: Gen.* 230 (2002) 137–151.
- [38] H. Matsuhashi, H. Shibata, H. Nakamura, K. Arata, *Appl. Catal. A: Gen.* 187 (1999) 99–106.
- [39] S.D. Rossi, G. Ferraris, M. Valigi, D. Gazolli, *Appl. Catal. A: Gen.* 231 (2002) 173–184.
- [40] R.D. Wilson, D.G. Barton, C.D. Baertsch, E. Iglesia, *J. Catal.* 194 (2000) 175–187.